Polarimetric Phased Array Calibration for Large-Scale Multi-Mission Radar Applications

Caleb Fulton and Jorge Salazar
Advanced Radar Research Center
The University of Oklahoma
Norman, OK

Dusan Zrnic, Djordje Mirkovic, Igor Ivic, and Dick Doviak
Cooperative Institute for Mesoscale Meteorological Studies
National Severe Storms Laboratory
Norman, OK

***Abstract*—Concepts for multi-mission weather and air traffic surveillance radar systems call for the use of large-scale phased array radar systems to meet practical beam flexibility and timeline requirements. While the individual air surveillance (defense) and air traffic missions have clear paths towards technical success using phased arrays, it has not yet been demonstrated that a large-scale phased array can meet the scientific needs of the dual polarization weather surveillance mission because there are inherent scan-dependent polarization biases in planar phased array radar systems. This paper highlights the challenges and potential technical solutions to the calibration and correction of these biases, summarizing current work towards the ultimate goal of demonstrating these techniques on a real system.**

Keywords—phased arrays; weather radar; calibration; dual polarization

I. Introduction to Overall Challenges

The US Multi-mission Phased Array Radar concept began more than a decade ago, with the goal being to replace the nation's air traffic control, air surveillance, and weather surveillance radar systems with a single network of advanced systems that would perform these missions with a single radar type [1]. More recently, there has been interest in relocating the DoD/DHS operated Air Route Surveillance Radars (ARSRs) from L band to another frequency; this effort is now called the Spectrum Efficient National Surveillance Radar (SENSR) program. The Government does not presume that SENSR will be a multi-mission radar, but the program's goals are at least consistent with this architecture. Throughout both program periods, the fundamental challenges have remained the same in that multi-mission capabilities and the timeline requirements associated with each mission virtually require that such a system (or even collection of systems) would take the form of a phased array. Therefore, cost comes into play in addition to an obvious difficulty in defining precise concepts of operation for such a multi-use (and multi-user) system. Proposed solutions in the past have included a large number of small X-band arrays that operate in a more distributed manner [2], but the conventional thought is that such a system would take the form of a large S-band array (either planar or cylindrical [3]), much like the current weather and air surveillance systems in size as well as locations throughout the country.

Regardless of the frequency, size, or even shape of such an array, the weather surveillance mission provides the additional fundamental challenge of replicating the scientific accuracy of a well-calibrated dish-based weather radar with a phased array. This is because, in general, both the shape and polarization characteristics of a phased array's patterns change as a function of scan angle, whereas those of a dish do not [4]. Table I summarizes the performance requirements that are derived from a notional SENSR weather mission; these requirements and their implications will be further explained in context throughout this paper. The beamwidth, sidelobe, and beam shape matching between polarizations (Ludwig-II AZ/EL is used for weather radar) can in principle be met through "traditional" phased array calibration and design principles (see [1] and references in [5]) that are more or less familiar to the overall large-scale phased array community. Some of these techniques are summarized in Fig. 1. However, *the strict polarization requirements pose new challenges, calling for new calibration steps* (highlighted in Fig. 1). At the time of writing, no large-scale system has demonstrated acceptable performance (outside of the principal planes [6]); this paper presents plans for increasingly-accurate correction on near-future large-scale systems, as shown in Fig. 2.

TABLE I. Summary of SENSR Requirements and Implications

Parameter	Specification	Implications/notes
AZ and EL beamwidths	1 deg.	Aperture > ~9m; large FF distance
Overall scan range (four-faced planar array assumed)	AZ +/- 45 deg; EL -1 to 20 deg. (with polarimetry), to 60 (other missions)	Intrinsic polarization must be "well-behaved" to 20 deg. EL
Close-in sidelobes	< -54 dBc (2-way)	Careful but traditional phased array calibration techniques must be used
Mid-range sidelobes	mask to -100 dBc at ±10 deg. (2-way)	
Far-out sidelobes	< -100 dBc (2-way)	
Bias in Z_{DR} estimate	**< 0.1 dB @ 0 dB Z_{DR}; 0.1Z_{DR}, Z_{DR} > 0.1 dB**	**Drives overall pol. requirements**
Bias in ρ_{HV} estimate	< 0.001	Additionally drives shape requirements
H/V beam peak match	**< 0.03 dB**	**Based on worst-case analysis**
H/V shape matching	**<0.5 dB @ -20 dBc**	**Preserves correlation**
Cross-polar isolation	**< -52/25 dBc for STSR/ATSR or PCSTSR; see Sec. II**	**At beam center, after correction (see text)**

In order for a modern weather radar to best identify types of precipitation, estimate rainfall rates accurately, and determine the effects of propagation on these measurements, dual

This work was sponsored by the US Spectrum Efficient National Surveillance Radar program through NOAA/NSSL and the FAA.

polarization is required. The principal measurements that drive the requirements are differential reflectivity (Z_{DR}), the ratio of the horizontal (H, or AZ) to vertical (V, or EL) returns, in power, at a given range/angle; ρ_{HV}, the correlation coefficient between H and V returns; and specific differential phase, K_{DP}, the derivative with respect to range of the phase difference between the H and V polarized returns [4]. Measurements of ρ_{HV} are corrupted by cross-polarization errors and beam shape mismatch, and degrade the ability to distinguish between different types of hydrometeors and between precipitation and insects, debris, dust, etc. Z_{DR} and K_{DP} are widely used for rainfall rate estimates [7]-[9] and satisfying the Z_{DR} accuracy requirement largely satisfies that on K_{DP}. Z_{DR} bias, in turn, is affected not only by mismatches in the H and V beam gains, but also by the existence of cross-polarization, leading to the last three requirements in the table (see Section IIa for details).

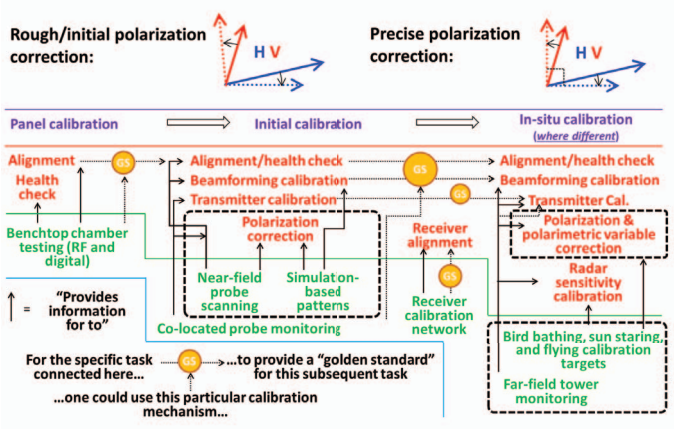

Fig. 1. Overall concept map for dual-pol phased array calibration (dotted boxes indicate the focus of this paper, those that are as yet not demonstrated).

The essential challenge in meeting these requirements is that phased arrays have inherent dependence of their polarization characteristics on scan angle. Ideal current sheets even have such scan dependencies, owing to geometrical effects in translating H and V electric currents to H and V radiated fields in the far field [10]. Patch antennas, common because of their low cost and relative ease of design, produce orthogonal fields only in the principal planes [11]. A slot-dipole combination (ideal electric and magnetic current sheets for V and H, respectively) –in principle having zero cross-polarization in this basis – will still have differences in the co-polar patterns as a function of scan [12], and any array tilt will lead to geometrically-induced cross-polarization for just about any array. Even cylindrical arrays, which can in principle maintain low cross-polarization due to symmetry arguments, have beam shape and pattern variance issues in practice [3]. Ultimately, some form of calibration and correction will be necessary to meet Table I's requirements [14].

Section II presents a high-level overview of the mathematics behind the measurement of the aforementioned polarimetric variables, providing a construct for its further discussion on the current theoretical correction process options. These correction techniques were first suggested in [4], simulated in [15] and [16], and further updated in [17], and will soon be applied to a number of large-scale testbeds, starting with the Advanced Technology Demonstrator (ATD) [1]. Until now, they have only been applied on small-scale systems ([18]) to the authors' knowledge. Section III presents a number of correction parameter estimation challenges and potential solutions within the context of these larger-scale demonstrators and practical measurement, simulation, and stability concerns. In particular, it discusses the prospect for the use of infinite array simulations, near-field (NF) measurements, and far-field (FF) verification to provide increasingly robust estimates of the radar's inherent scan-dependent polarization characteristics at beam center, from simulations and nearfield measurements through far-field verification (as motivated by the highlights in Fig. 1). Finally, future prospects are discussed in the Conclusion section.

II. Summary of Polarization Correction Processes and Tradeoffs

A. Basic Signal Model and Raw Data Corrections

In its simplest form, one can write the returns from a pulse at range r for a dual-pol radar in vector form as:

$$\mathbf{V} = C(r)\oiint_S \mathbf{R}^{\mathrm{T}}(\Omega,\Omega_S)\mathbf{S}(r,\Omega)\mathbf{T}(\Omega,\Omega_S)\mathbf{A}\,d\Omega\,, \qquad (1)$$

where $\mathbf{A} = [A_a\ A_b]^{\mathrm{T}}$ are the complex H and V pulse weights into the radar ports "a" and "b" (nominally leading to H and V radiation, respectively), $\mathbf{S}$ is the effective 2x2 scattering matrix at range r and space angle pair Ω (AZ and EL, here) that relates the incident H and V waves to the scattered H and V waves, including polarization-related propagation effects, $C(r)$ is an overall propagation term that is irrelevant for the polarization discussion, $\mathbf{V} = [V_a,\ V_b]^{\mathrm{T}}$ for receive ports "a" and "b", and $\mathbf{T}$ and $\mathbf{R}$ are 2x2 matrices containing the effective radiation patterns at the scan angle pair Ω_S. For example (subscripts are the same for $\mathbf{R}$):

$$\mathbf{T}(\Omega,\Omega_S) = \begin{bmatrix} T_{aH}(\Omega,\Omega_S) & T_{bH}(\Omega,\Omega_S) \\ T_{aV}(\Omega,\Omega_S) & T_{bV}(\Omega,\Omega_S) \end{bmatrix}. \qquad (2)$$

As detailed in [15], this *polarimetric pattern* is only approximately equal to an element factor $\mathbf{E}(\Omega)$ that is inherent to the element, multiplied by an array factor $AF(\Omega,\Omega_S)$ that describes the phased array scanning. An example is illustrated in Fig. 2 for the "sandbox" array in Section III; these patterns are actually quite similar to those often seen in the patch-based radiators that are being used in the ATD and other demonstrators [1], [11], [15]. Importantly, $\mathbf{T}$ and $\mathbf{R}$ take into account all of the non-ideal effects described in Section III (such as errors in the T/R modules), not just the factor $\mathbf{E}$.

The radar operates by sending out multiple pulses ($\mathbf{A}_1$, $\mathbf{A}_2$, etc.) and processing the resulting returns. Ideally, near the scan angle both $\mathbf{T}$ and $\mathbf{R}$ are proportional to the identity matrix, so that the N^{th} pulse return is proportional to $\mathbf{SA}_N$. Unfortunately, due to polarization errors, this is not the case in general, and some form of correction is required [14]. The radar can either operate in simultaneous transmission, simultaneous receive (STSR) mode ($\mathbf{A} = [1\ A]^{\mathrm{T}}$), assuming that $\mathbf{S}$ is diagonal, or in alternating transmission, simultaneous

receive (ATSR) mode, where pulse pairs $\mathbf{A}_1 = [1\ 0]^T$ and $\mathbf{A}_2 = [0\ 1]^T$ alternatively probe the weather in the H and V polarizations. For simplicity, denote a received 2x1 STSR vector as $\hat{\mathbf{S}}_{STSR}$ and effective received 2x2 ATSR matrix (juxtaposed received vectors) as $\hat{\mathbf{S}}_{ATSR}$. One idea for correction of **T** and **R** errors is that if one knows the values of **R** and **T** near the beam peak for a given scan angle, one could "un-do" their polarization errors in the ATSR case by calculating

$$\widetilde{\mathbf{S}}_{ATSR} = \mathbf{C}_{\mathbf{R}}(\Omega_S)\hat{\mathbf{S}}_{ATSR}\mathbf{C}_{\mathbf{T}}(\Omega_S), \tag{3}$$

where $\mathbf{C}_{\mathbf{T}}(\Omega_S) = \mathbf{T}(\Omega_S,\Omega_S)^{-1}$ is the correction matrix for transmit errors and $\mathbf{C}_{\mathbf{R}}(\Omega_S) = \mathbf{R}^{\mathrm{T}}(\Omega_S,\Omega_S)^{-1}$ is the correction matrix for receive. These matrices, the inverses of the polarimetric patterns at beam center for a given scan angle, effectively make the products $\mathbf{C_R R}^T$ and $\mathbf{TC_T}$ proportional to the identity matrix at scan center. An example of one such product is shown in the bottom of Fig. 2. Analogous processing for STSR forms $\widetilde{\mathbf{S}}_{STSR} = \mathbf{C}_{\mathbf{TR}}(\Omega_S)\hat{\mathbf{S}}_{STSR}$, where

$$\mathbf{C}_{\mathbf{TR}} = \begin{bmatrix} (T_{aH} + AT_{bH})^{-1} & 0 \\ 0 & (T_{aV} + AT_{bV})^{-1} \end{bmatrix}\mathbf{C}_{\mathbf{R}} \tag{4}$$

for a given value of A, and again the T_{xY} are evaluated at the beam center for a given Ω_S.

In large arrays, it has been shown that despite the integral nature of (1), these "beam-center" corrections are sufficient to meet accuracy requirements [15]-[16]. This has largely been concluded in the context of rigorous simulations of biases in the polarimetric variable estimates – particularly Z_{DR} – under a variety of assumptions. For the purposes of discussion, a simple evaluation of such a bias is:

$$Z_{\mathrm{DRb}} = \frac{\oiint_S \left| R_{aH}(T_{aH} + AT_{bH}) + e^{j\Phi_{DP}} R_{aV}(T_{aV} + AT_{bV}) \right|^2 d\Omega}{\oiint_S \left| R_{bH}(T_{aH} + AT_{bH}) + e^{j\Phi_{DP}} R_{bV}(T_{aV} + AT_{bV}) \right|^2 d\Omega} \tag{5}$$

for STSR and

$$Z_{\mathrm{DRb}} = \frac{\oiint_S \left| R_{aH}T_{aH} + e^{j\Phi_{DP}} R_{aV}T_{aV} \right|^2 d\Omega}{\oiint_S \left| R_{bH}T_{bH} + e^{j\Phi_{DP}} R_{bV}T_{bV} \right|^2 d\Omega} \tag{6}$$

for ATSR. Here, the patterns are "effective" patterns after any use of (3) or (4) [15] and Φ_{DP} is the cumulative differential propagation/back-scattering phase between H and V along the path to an ideal volume where **S** is proportional to the identity matrix (i.e., assuming spherical scatterers).

Several important points emerge from such an analysis. The bias is dependent on Φ_{DP}, in general, and the worst-case results should be considered. In both cases, if **R** is similar to **T**, then the co-polar terms appear to the fourth power, overall, and this drives the extreme requirement in Table 1 for co-polar matching. For ATSR, cross-polarization terms appear at most as *second-order*, whereas for STSR they are *first-order*; this is why the cross-pol requirements are so much more stringent in the latter case. *Importantly, STSR is strongly preferred over ATSR* because the latter suffers from decorrelation of returns between pulses in addition to unacceptable Doppler and differential phase ambiguities [12]-[13]. Thus, any additional techniques that help mitigate such strict cross-polarization requirements would be helpful. One important result is that if the cross-polar pattern is shaped "co-axially" as in the bottom of Fig. 2, each of the either two or four "lobes" tends to be 180 deg. from an adjacent lobe and, under the integral in (5), its contributions cancel out. Such lobes can be as high as -26 dBc [19] while still satisfying requirements, so long as the beam center is ideally compensated. Before addressing how the $\mathbf{C_T}$, $\mathbf{C_R}$, and $\mathbf{C_{TR}}$ matrices may be measured (Section III), the following subsections discuss additional measures that may help alleviate the strict -52 dBc cross-pol requirement or provide alternative correction mechanisms.

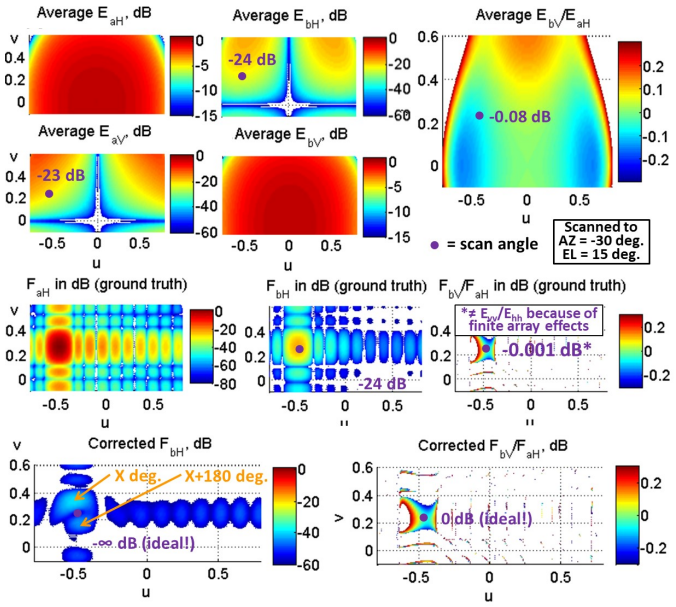

Fig. 2. Pattern-based correction process: (top) Embedded element pattern and ratio of E_{aH} to E_{bV}, (middle) Uncorrected radiation patterns (H excitation), and (bottom) Corrected H radiation pattern. Note: The direction cosines u and v map as u = sin(AZ)cos(EL) and v = sin(EL).

B. *Phase Coding for Cross-Polar Isolation*

Phase coding between pulses has been proposed [20], evaluated [21] and experimentally tested [22] as a means for reducing the impact of cross coupling. Its operation is best explained in the context of a basic example of weather signal processing; take, for example, an estimator of H power assuming 0 dB Z_{DR} and $\rho_{HV} = 1$ ($\mathbf{S} = S_H\mathbf{I}$, $\mathbf{I}$ = identity matrix):

$$\hat{S}_H \propto \left\langle |V_a|^2 \right\rangle \propto \langle \text{numerator of (5)} \rangle = \sum_{n=1}^{N} (D + E + F + G). \tag{7}$$

The four terms in the sum vary both in their physical meaning and in how they depend on the phase code $A[n]$ from pulse to pulse. The leading term $D = |R_{aH}T_{aH}|^2$ is the ideal output which, in ratio with the denominator of (5)'s ideal output of $|R_{aV}T_{aV}|^2$, would lead to a value of 0 dB for (5) under perfect co-polar matching and zero cross-polarization. Next,

$$E = 2\,\mathrm{Re}\left\{e^{j\Phi_{DP}} R_{aH}^{*} T_{aH}^{*} R_{aV} T_{aV}\right\} + \left|R_{aV} T_{aV}\right|^{2} \tag{8}$$

is a term that also appears under ATSR operation, and contains at worst second-order cross-pol. terms. The last two terms in (7) depend on the phase coding $A[n]$, and are specific to STSR:

$$F = 2\,\mathrm{Re}\left\{A[n]\left(R_{aH}^{*} T_{aH}^{*} + e^{j\Phi_{DP}} R_{aV} T_{aV}\right)\times \left(R_{aH}^{*} T_{bH}^{*} + e^{j\Phi_{DP}} R_{aV} T_{bV}\right)\right\} \tag{9}$$

contains the first-order cross-polar terms that plague normal STSR operation, but under the summation in (7) will disappear when $A[n] = (-1)^n$, or some other code that sums to zero over a collection of pulses; this is the primary achievement of phase coding in helping to enable STSR, and effectively reduces the requirement for cross-pol to that of ATSR. The last term

$$G = \left|A[n]\left(R_{aH} T_{bH} + e^{j\Phi_{DP}} R_{aV} T_{bV}\right)\right|^{2}, \tag{10}$$

also at worst second-order in terms of cross-pol, does not get removed in (7) through averaging. However, in terms of the Doppler spectrum of the returns, this term ends up being separated from the main term in Doppler by half the Nyquist rate. If the spectrum width of the returns is less than this separation, then G's contribution can be filtered out during preprocessing. In summary of the most recent analysis in [23], phase coding effectively removes first-order cross-polar terms, reducing cross-pol requirements to those of ATSR; however, it has limitations whereas it tends to lower (bias) the estimates of ρ_{HV} if cross-pol is high. Nevertheless, it remains the simplest means by which cross-pol requirements can be significantly reduced under the desirable STSR operation, leading to co-polar gain mismatch being the largest source of error for Z_{DR}.

C. Product-Level Corrections and Other Options

There are other options besides the matrix-based "raw data" corrections of (3) or (4) for mitigating biases due to polarization errors. One approach is to first form the second-order estimates of $\langle|V_a|\rangle^2$, $\langle|V_b|\rangle^2$, and $\langle V_a^{*} V_b\rangle$ based on un-corrected raw data, leading to a set of equations that are complex linear functions of the desired un-biased estimates as well as the entries of the **R** and **T** matrices in (1). In principle, these equations could be solved to retrieve the un-biased second-order estimates, from which the polarimetric variables could be computed. This approach has the advantage of requiring fewer computational resources than the sample-by-sample processing of (3) or (4), but still requires knowledge of at least the beam-center values of **R** and **T** for each scan angle of interest. For an early example of such a scheme, see [23].

There are also concepts for *correction-free* polarimetry that seek to find compromises in different scan regions that exploit the inherent properties of well-designed radiators, such as the patch antenna in [11]. For example, in lower elevation scans (EL < a few deg.), it may be possible to perform STSR with long PRTs using such an antenna, since cross-polarization is so low (assuming low coupling through hardware components). For higher elevations, either phase coding or ATSR could be used, with higher PRTs (to mitigate ambiguities) to achieve acceptable performance (assuming the cross-polar isolation can be kept below -25 dB). Importantly, these concepts only address the impact of cross-pol on performance, not co-polar gain mismatches. Inherently, the best solution will at least include corrections for mismatches in co-polar patterns, while carefully maintaining beam shape matching for each scan angle of interest. The following section discusses the overall approaches to estimating both co-polar mismatches and, if necessary, cross-polar patterns for use in the more sophisticated correction techniques outlined above.

III. Polarimetrtic Pattern Estimation: Challenges and Potential Solutions

The extent to which the polarimetric patterns **T** and **R** inherit beam-center values that are directly predictable by **E** is limited by non-ideal phased array behavior. Some of these are predictable or, in principle, could be simulated, while others demand verification through direct measurement. In both cases, there are open questions as to how to use increasingly accurate estimation techniques to provide the post-correction accuracies of Table I, and to do so with a minimally-dense grid of beam center correction points. This section summarizes the current approaches being taken with near-future demonstrators.

A. Simulation-Based Approaches

In an infinitely large array, Floquet's theorem dictates that each element's radiation pattern $\mathbf{E}_n$ varies only by a phase shift associated with its displacement $\boldsymbol{r}_n$ from array center, such that $\mathbf{E}_n(\Omega) = \mathbf{E}(\Omega) e^{j\mathbf{k}(\Omega)\bullet\mathbf{r}_n}$, $\mathbf{k}(\Omega)$ being the propagation vector. This can be exploited for large arrays through *unit cell* numerical simulations, leading to accuracies for most elements on the order of 0.1 dB through subsequent application of the aforementioned $AF(\Omega,\Omega_S)$ array factor [24]; it is the default, practical approach used for analysis of most demonstrators. However, even if such an approach perfectly captures the geometry and materials of the radiator, it is limited by the following errors, *even with ideal phased array electronics*:

1) *Finite array effects:* The classic limitation of the approach is that it does not accurately capture the behavior of elements near the edge of the array, which experience a different mutual coupling environment and contribute to edge diffraction effects. While more rigorous "hybrid mode" (a mix of finite and infinite array) analysis has shown that beam-center polarization of larger arrays is practically unaffected by these issues (see [15]), in order for simulations to be trusted as being reflective of reality during the design process one must verify performance in as large a finite array as possible. Fig. 3 shows recent measurements to verify one of the central $\mathbf{E}_n$ patterns in an 8x8 subarray of the ATD relative to a finite array simulation of said subarray. Fig. 4 shows an averaged $\mathbf{E}_n$ measurement of the central 4x4 sector of an 8x8 subarray of the element in [11], compared to an infinite array simulation. In both cases, agreement is reasonable, but is perhaps insufficient to be used as the sole basis for achieving Table I's accuracies.
2) *Manufacturing tolerance issues*: One must of course be concerned with variance in dimensions and material properties in a large array. For the ATD, this was

investigated very briefly, and was found to contribute no worse to polarization issues than typical array electronics.

3) *Ground plane gaps:* Gaps are often required between the ground planes of adjacent subarrays; this is indeed the case for the ATD. Recent analysis has shown that while this may limit the ability to achieve 100 dB+ two-way peak side (grating) lobes, it is not a primary error source in beam-center polarization [25].

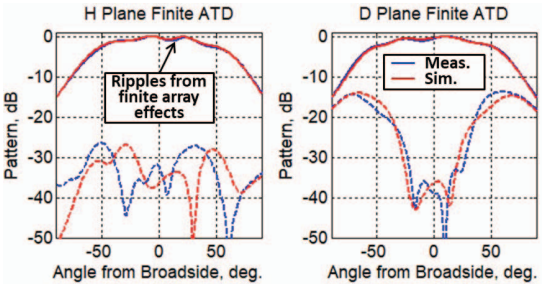

Fig. 3. Far-field measurement vs. simulation for one of the central elements of an 8x8 panel from the ATD, for the H plane (E plane similar) and D plane.

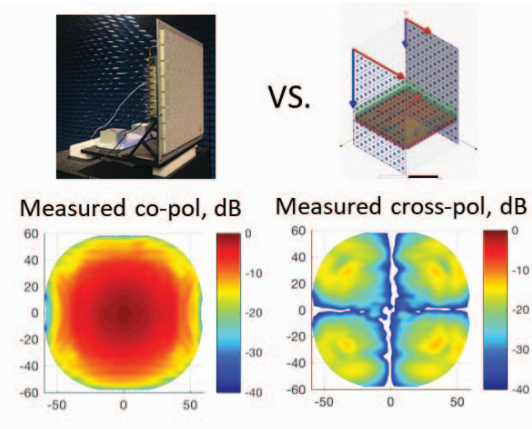

Fig. 4. Near-field measurement of an 8x8 OU Horus panel: average embedded element pattern from the ccenter of an 8x8 array vs. an infinite array simulation in Ansys HFSS (now being processed at the OU ARRC).

B. *Large-array measurement-based approaches*

Ultimately, the most effective method for realizing the correction processes outlined in Section II will be based on measurements whenever possible, realizing the "precise" correction shown in Fig. 2. There are additional effects that measurements capture, and this will allow for increasingly precise correction during NF and FF measurements.

1) *Additional effects:* Pure simulations, or even predictions based on separate measurements, will struggle to accurately capture several real-world effects. These include active impedance effects on transmit, element failures that may systematically affect H differently than V, the effects of ground reflections on far-field radiation, any systematic variations with temperature, radome effects [26], and more. In principle, very careful NF or FF measurements can provide the 100ths of dB levels of accuracy dictated by Table I [27].

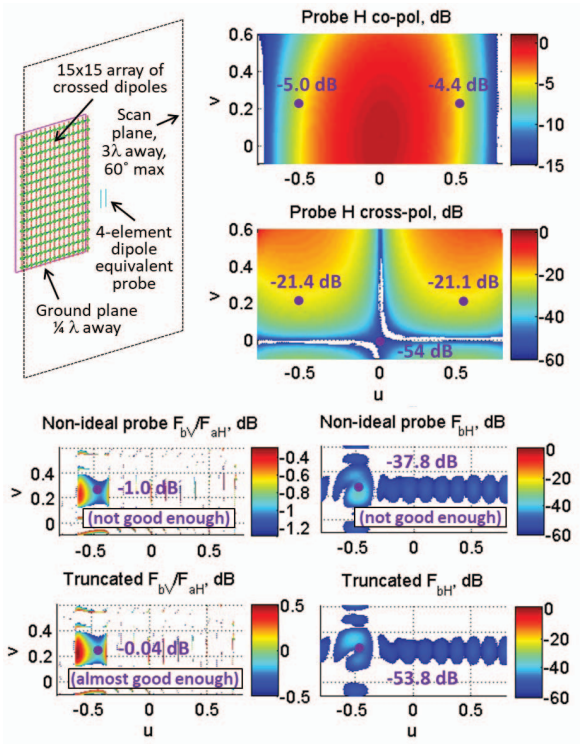

Fig. 5. Near-field Sandbox and example result with non-ideal probe correction and with truncation issues, showing resulting errors after correction

2) *NF-FF issues*: NF measurements, usually used for initial calibration (Fig. 1) can in principle provide polarization correction as well. To understand the impact of probe polarization correction and other effects, a simple "sandbox" has been developed to simulate the ground-truth electromagnetics, using the induced EMF method to capture all coupling effects [28]. Here, an array of 0.48 λ long, 0.5 λ-spaced crossed-dipoles that are 0.25 λ away from an infinite ground plane has been analyzed. Fig. 5 shows example results for 15x15 elements with a probe that exhibits the slight asymmetries that are present in most NF probes (here, the probe is rotated by 0.1 deg. one of the equivalent dipoles is shifted vertically by 0.1 λ). If an ideal probe model is used, or if the scan plane is truncated from a 60 deg. equivalent field of view to 45 deg., there can be limitations to the accuracy of the resulting corrections, as indicated in the figure. Current ATD plans are to use precise probe measurements and traditional matrix-based correction in the u-v (direction cosine) domain, of the same form as the $\mathbf{C}_R\mathbf{R}^T$ product in (3) for this function.

3) *Future Tools:* A FF tower will be installed 425m from the ATD and, through multi-axis rotation of the array, this will allow for FF polarization characterization that will hopefully deliver the accuracies of Table I. This will also be used to corroborate recent NF ATD measurements [29]. A future system is also under development that will use a probe installed on a UAV as a means to obviate the need for multi-axis array rotation, an obvious issues for a future SENSR implementation [30]. Fig. 6 shows early progress towards efforts to deliver a UAV prototype with an absorber-shielded sensor on a 3-axis gimbal that can

measure FF radiation with the accuracies of Table I, with GPS guidance to coordinate radar pattern collection.

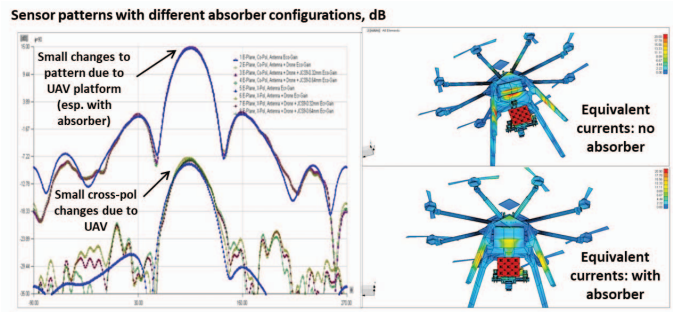

Fig. 6. UAV-based calibration: (left) patterns of sensor embedded with UAV, and (right) absorber-based treatment of UAV for enhanced accuracy.

IV. Future Outlook and Conclusions

This paper has provided an update to [17] on current efforts towards realizing practical phased array weather radar polarimetry by combining simulation, measurement, and waveform processing techniques. As more is learned in the coming years through experimental validation of these techniques and concepts, the community will gain a better understanding of the true costs and benefits associated with the specific requirements of Table I. In fact, there is already a changing philosophy as to whether the 0.1 dB requirement on Z_{DR} bias (a principal driver) can be relaxed, given that K_{DP} is increasingly the primary factor for rainfall rate estimation in modern processing schemes; however, 0.1 dB accuracies are still required for discrimination between warm (wet) snow and cold (dry) snow [31]. The use of correction techniques on the ATD and other larger-scale demonstrators will help clarify the overall engineering trade space as it relates to priorities for a notional SENSR's service and scientific missions.

Acknowledgment

The authors would like to acknowledge the contributions of numerous engineers, students, scientists, and administrators who have supported these developments over the last decade.

References

[1] J. Stailey and K. Hondl, "Multifunction Phased Array Radar for aircraft and weather surveillance," *Proc. IEEE,* 104(3), March 2016.

[2] D. McLaughlin, E. Knapp, Y. Wang, and V. Chandrasekar, "Distributed weather radar using X-band active arrays," *IEEE Radar Conf.*, 2007.

[3] C. Fulton et al., "Cylindrical Polarimetric Phased Array Radar (CPPAR): beamforming and calibration for weather applications," *IEEE Trans. on Geoscience and Remote Sensing*, 55(5), 2017.

[4] G. Zhang, et al., "Phased array polarimetry for weather sensing: a theoretical formulation for bias corrections," *IEEE Trans. Geosci. Remote Sens*. 47(11), 2009.

[5] C. Fulton, M. Yeary, D. Thompson, J. Lake, and A. Mitchell, "Digital phased array systems: challenges and opportunities," *Proc. IEEE*, 104(3) 2016.

[6] R. Medina, J. Salazar, E. Knapp, and D. McLaughlin, "Calibration and validation of the CASA phased array antenna," *2012 European Radar Conference*, 2012.

[7] D. Zrnić, R. Doviak, G. Zhang, and R. Ryzhkov. "Bias in differential reflectivity due to cross coupling through the radiation patterns of polarimetric weather radars," *J. Atmos. Oceanic Technol.*, 27(10), 2010.

[8] M. Hudlow, R. Farnsworth, and P. Anhert, "NEXRAD technical requirements for precipitation estimation and accompanying economic benefits," *Hydro Technical Note 4, Office of Hydrology, NOAA*, 1983.

[9] Y. Wang and V. Chandrasekar, "Polarization isolation requirements for linear dual-polarization weather radar in simultaneous transmission mode of operation," *IEEE Trans. on Geosci. Remote Sens,* 44(8), 2006.

[10] A. Boryssenko, "Polarization constraints in dual polarized phased arrays derived from an infinite current sheet model," *IEEE Ant. and Wireless Prop. Letters*, 8, 2009.

[11] J. Diaz et al., er, "A dual-polarized stacked patch antenna with wide-angle and low cross-polarization for fully digital MPAR," *2016 IEEE Intl. Symp. on Phased Array Systems and Tech.*, 2016.

[12] D. Zrnić, V. Melnidov, and R. Doviak, "Issues and challenges for polarimetric measurement of weather with an agile beam phased array radar," *NOAA/NSSL report*, 2012.

[13] M. Melnikov, D. Zrnić, "On the alternate transmission mode for polarimetric phased array weather radar," *J. Atmos. Oceanic Technol.,* 32, 2015.

[14] D. Zrnic, G. Zhang, and R. Doviak, "Bias correction and Doppler measurement for polarimetric phased array radar." *IEEE Trans. Geosci. Remote Sens.*, 49(2), 2011.

[15] C. Fulton and W. Chappell, "Calibration of panelized polarimetric phased array radar antennas: a case study," *2010 IEEE Intl. Symp. on Phased Array Systems and Tech.,* 2010.

[16] C. Pang et al., "Polarimetric bias correction of practical planar scanned antennas for meteorological applications, *IEEE Trans. Geosci. Remote Sens.*, 54(3), 2016.

[17] C. Fulton, J. Herd, S. Karimkashi, G. Zhang, and D. Zrnic, "Dual-polarization challenges in weather radar requirements for Multifunction Phased Array Radar," *2013 IEEE Intl. Symp. on Phased Array Systems and Tech.*, 2013.

[18] C. Fulton and W. Chappell, "Calibration of a digital phased array for polarimetric radar," *2010 IEEE MTT-S Intl. Microwave Symp*., 2010.

[19] S. Bhardwaj and Y. Rahmat-Samii, "Revisiting the generation of cross-polarization in rectangular patch antennas: A near-field approach," *IEEE Ant. Prop. Mag.,* 56(1), 2014.

[20] D. Zrnić, R. Doviak, V. Melnikov, and I. Ivić, "Signal design to suppress coupling in the polarimetric phased array radar. *J. Atmos. Oceanic Technol.*, *31(5)*, 2014.

[21] I. Ivić, "Phase code to mitigate the copolar correlation coefficient bias in PPAR weather radar," *IEEE Trans. Geosci. Remote Sens.*, 55(4), 2017.

[22] I. Ivić, "An experimental evaluation of phase coding to mitigate the cross-coupling biases in PPAR," *38th Intl. Conf. on Radar Met.*, 2017.

[23] I. Ivić, "Options for polarimetric variable measurements on the MPAR Advanced Tech. Demonstrator," *2018 IEEE Radar Conf., 2018.*

[24] E. Brookner et al., "Demonstration of accurate prediction of PAVE PAWS embedded element gain," *2010 IEEE Intl. Symp. on Phased Array Systems and Tech.*, 2010.

[25] L. Bhowmik and C. Fulton, "Analysis and measurement of grating lobe effects in infinite planar arrays of finite-sized subarrays," *2016 IEEE Intl. Symp. on Phased Array Systems and Tech.,* 2016.

[26] J. Salazar, P. Siquiera, J. Trabal, E. Knapp, and D. McLaughlin, "Performance of the wet radomes for phased array weather radars: evaluation and applications," 2012 European Radar Conference, 2012.

[27] O. Breinbjerg, S. Pivnenko, O. Kim, and J. Nielsen, "Recent advances in antenna measurement techniques at the DTU-ESA spherical near-field antenna test facility," *Proc. 31st URSI GASS*, 2014.

[28] C. Balanis, "Antenna Theory: Analysis and Design, 4th ed." *Wiley*, 2016.

[29] D. Conway, D. Russel, A. Morris, and C. Parry, "Multifunction Phased Array Radar Advanced Technology Demonstrator nearfield test results," *2018 IEEE Radar Conf.*, 2018.

[30] C. Boyer and C. Fulton, "UAV-based calibration for polarimetric phased array radar," (poster) *16th Annual AMS Student Conference*, 2017.

[31] A. Ryzhkov and D. Zrnic, "Discrimination between rain and snow with a polarimetric radar," *Jour. Appl. Meteor*., 37, 1998.